Molecular Cell
Article

Polycomb-Dependent H3K27me1 and H3K27me2 Regulate Active Transcription and Enhancer Fidelity

Karin J. Ferrari,[1,3] Andrea Scelfo,[1,3] SriGanesh Jammula,[1,3] Alessandro Cuomo,[1] Iros Barozzi,[1] Alexandra Stützer,[2] Wolfgang Fischle,[2] Tiziana Bonaldi,[1] and Diego Pasini[1,*]
[1]Department of Experimental Oncology, European Institute of Oncology (IEO), Via Adamello 16, 20139 Milan, Italy
[2]Laboratory of Chromatin Biochemistry, Max Planck Institute for Biophysical Chemistry, 37077 Göttingen, Germany
[3]These authors contributed equally to this work
*Correspondence: diego.pasini@ieo.eu
http://dx.doi.org/10.1016/j.molcel.2013.10.030

SUMMARY

H3K27me3 is deposited at promoters by the preferential association of Polycomb repressive complex 2 (PRC2) with CpG-rich DNA elements regulating development by repressing gene transcription. H3K27 is also present in mono- and dimethylated states; however, the functional roles of H3K27me1 and H3K27me2 deposition remain poorly characterized. Here, we show that PRC2 activity is not only associated with H3K27me3 but also regulates all forms of H3K27 methylation in a spatially defined manner, contributing to different genomic functions in mouse embryonic stem cells. H3K27me1 accumulates within transcribed genes, promotes transcription, and is regulated by Setd2-dependent H3K36me3 deposition. Contrarily, H3K27me2 is present on approximately 70% of total histone H3 and is distributed in large chromatin domains, exerting protective functions by preventing firing of non-cell-type-specific enhancers. Considering that only 5%–10% of deregulated genes in PRC2-deficient cells are direct H3K27me3 targets, our data support an active role for all H3K27 methylated forms in regulating transcription and determining cell identity.

INTRODUCTION

The acetylation (ac) and methylation (me) of histone lysine (K) residues play differential roles in regulating gene expression. Although acetylation correlates with active transcription, lysine methylation promotes either activation or repression of gene expression depending on the target residue and the level of its acquired methylation (Berger, 2007; Kouzarides, 2007). H3K27 trimethylation (me3) plays a role in maintaining gene transcriptional repression, and it is deposited preferentially at CpG-dense promoters by the lysine methyltransferase (KMT) activity of the Polycomb repressive complex 2 (PRC2) (Morey and Helin, 2010). The SET-domain-containing proteins EZH2 and EZH1 mediate H3K27 methylation but require the formation of a catalytically active PRC2 complex that includes the Polycomb group (PcG) proteins Suz12 and Eed (Cao and Zhang, 2004; Pasini et al., 2004).

H3K27me3 deposition serves as a docking site for the recruitment of PRC2 and Cbx-containing PRC1 complexes (Morey and Helin, 2010). Importantly, Eed directly binds H3K27me3, suggesting a self-maintaining, DNA-independent mechanism for PRC2 association with target sites (Hansen et al., 2008; Margueron et al., 2009). All subunits of the PRC2 complex are essential for embryonic development. A loss of Eed, Ezh2, or Suz12 results in severe defects during gastrulation that are consistent with the role of PRC2 in repressing genes involved in lineage specification (Bracken and Helin, 2009). The mechanisms of PRC2 recruitment to DNA are still poorly understood. In *Drosophila melanogaster*, this occurs via transcription factor (TF) recognition of specific DNA sequences, known as the Polycomb response elements (PREs) (Ringrose et al., 2003; Simon and Kingston, 2009; Sing et al., 2009); however, such mechanisms do not seem to be generally conserved in mammals. Indeed, the only homolog of the TFs that mediates PcG recruitment to PREs in flies, YY1 (Pho in *Drosophila*), does not have a general role in PRC recruitment in mammalian cells (Mendenhall et al., 2010; Vella et al., 2012). Although two distinct DNA elements have been proposed to retain PRE-like activities in mice, several additional mechanisms were shown to mediate PcG recruitment at gene promoters in mammalian cells. This involves interactions with different transcription factors or with noncoding RNAs or proceeds by sensing the transcriptional state of CpG-rich genomic regions (Morey and Helin, 2010). Other proteins, such as the Jumonji and ARID-domain-containing protein Jarid2, the zinc finger protein AEBP2, and the PHD-containing proteins PHF1, MTF2, and PHF19 (Aloia et al., 2013; Margueron and Reinberg, 2011), have been identified as additional components of the PRC2 complex that exert different regulatory functions but are not required for its intrinsic KMT activity. Finally, H3K27me3 deposition stimulates the recruitment of Cbx-containing PRC1 complexes, thus regulating histone H2A monoubiquitylation and stable gene silencing via the inhibition of RNA polymerase II (RNAPII) activation (Di Croce and Helin, 2013).

Several reports have shown that PRC2 also controls other forms of H3K27 methylation. Although PRC2 activity is required for the H3K27me2 in different cells (Pasini et al., 2007), its role in regulating H3K27me1 is still a matter of debate (Margueron et al., 2008; Shen et al., 2008). The analysis of

PRC2 KMT activity showed a high conversion rate in generating H3K27me1 and H3K27me2 products, whereas further conversion to H3K27me3 occurs with a 10-fold reduced kcat, suggesting that H3K27me0 and H3K27me1 are better substrates for PRC2 activity in vitro than H3K27me2 (McCabe et al., 2012). In addition, although previous studies have identified typical genome-wide distribution patterns for H3K27 methylation, linking the H3K27me1 to active genes (Cui et al., 2009; Steiner et al., 2011; Vakoc et al., 2006), little is known about the contribution of PRC2 activity for the distribution and regulation of these modifications throughout the genome.

Here, we provide a genome-wide functional characterization of PRC2-dependent H3K27me1 and H3K27me2 in mouse embryonic stem cells (ESCs). We show that the three forms of H3K27 methylation are mutually exclusive and form spatially defined genomic domains. Although H3K27me1 accumulates specifically in intragenic regions of actively transcribed genes and correlates with H3K36me3 deposition, H3K27me2 forms large intergenic and intragenic domains. Importantly, we show that genome-wide intragenic deposition of H3K27me1 is dependent on PRC2 activity and that its loss correlates with impaired transcription. Furthermore, we show that PRC2 enzymatic activity is influenced by adjacent H3K36me3 deposition, determining a preferential accumulation of H3K27me1 with respect to H3K27me2. Finally, we provide evidence that the broad deposition of H3K27me2 could serve as a protective mechanism from unspecific H3K27 acetylation that prevents cells from firing non-cell-type-specific enhancers. Notably, our data identify additional mechanisms of PcG-mediated transcriptional control that involve both active gene transcription and enhancer regulation.

RESULTS

PRC2 Controls Distinct H3K27 Methylation Domains

In a previous proteomic study aimed at characterizing changes in histone posttranslational modifications (PTMs) induced by the loss of PRC2 activity, we determined the relative abundance of several histone H3 PTMs in mouse ESCs (Jung et al., 2010). This analysis revealed that H3K27 is found in different methylated forms that correspond to more than 80% of the total histone H3. In contrast, unmodified H3K27 represents on average 16% of the total H3, whereas H3K27ac is restricted to approximately 2% (Figure 1A). Furthermore, these data unveiled that, in mouse ESCs, more than 70% of H3K27 is present in its dimethylated form (H3K27me2), whereas 7% and 4% of total H3 is in the H3K27me3 and H3K27me1 forms, respectively (Figure 1A). Moreover, H3K27me3 showed a preferential accumulation in the H3.3 variant that is consistent with its deposition at promoter regions of both silent and expressed genes (Goldberg et al., 2010). Overall, these data reveal that the vast majority of histone H3K27 in mouse ESCs is posttranslationally modified, H3K27me2 being present as the most abundant modification.

Our previous proteomic studies demonstrated that the levels of all three forms of H3K27 methylation are reduced in *Suz12* knockout (KO) mouse ESCs (Jung et al., 2010). Consistent with this, western blot analyses of extracts prepared from independent *Ezh2*, *Eed*, and *Suz12* KO mouse ESC lines or from mouse ESCs that expressed *Eed*-specific small interfering RNAs (shRNAs) (Figure S1A available online) showed that the inhibition of PRC2 activity induced a global loss of H3K27me3 and H3K27me2 and a significant reduction of H3K27me1 levels (Figures 1B, S1B, and S1C). This reduction was not a consequence of the loss of activity of G9a and Glp, two H3K9 KMTs that were recently shown to target H3K27 in vivo (Tachibana et al., 2005; Wu et al., 2011). No changes in expression levels for either G9a or Glp were seen in *Eed* KO mouse ESCs (Figure S1D), and the direct loss of G9a and Glp activity did not change H3K27 methylation levels in ESCs (Figures S1E and S1F).

To explore the genome-wide distribution of the different forms of H3K27 methylation, we performed chromatin immunoprecipitation (ChIP) analyses coupled to high-throughput DNA sequencing analyses (ChIP-seq) using antibodies specific for H3K27me1, H3K27me2, H3K27me3, and total H3 in mouse ESCs (Figure 1C). The specificity of the antibodies was tested with different sets of modified peptides, highlighting the specificity among different sites of methylation and among the different methylation states of the same residue (Figures S1G–S1J). The genomic snapshots of these analyses showed that the different methylated forms of H3K27 are deposited in mutually exclusive genomic domains (Figure 1C). Moreover, although H3K27me2 was spread across intergenic and intragenic regions, H3K27me1 preferentially accumulated within gene bodies (Figure 1C). In addition, the comparison with ChIP-seq results for H3K36me3 (Mikkelsen et al., 2007) showed a striking overlap between H3K27me1 and H3K36me3 deposition at the same intragenic sites (Figure 1C). Finally, correlative analyses of the intragenic signals for H3K27me2, H3K27me1, and H3K36me3, relative to all RefSeq annotated genes, demonstrated that, although H3K27me2 negatively correlated with H3K27me1 and H3K36me3 deposition, the accumulation of H3K27me1 positively correlated with H3K36me3 (Figures 2A and 2B). Such deposition patterns were not a consequence of active H3K27 demethylation, given that neither the knockdown of the H3K27 demethylases *Utx* and *Jmjd3* nor the global inhibition of intracellular demethylases activity through hypoxia induction by $CoCl_2$ treatment affected the global and site-specific H3K27 methylation levels (Figure S2). Given that PRC2 was found to be associated preferentially with regions of H3K27me3 accumulation (Boyer et al., 2006; Bracken et al., 2006; Lee et al., 2006; Mendenhall et al., 2010), our results strongly suggest that H3K27me1 and H3K27me2 deposition takes place in the absence of a stable association of PRC2 with these genomic regions.

Given that H3K36me3 is a modification linked to gene transcriptional elongation (Kizer et al., 2005; Li et al., 2003; Li et al., 2002; Xiao et al., 2003), we divided all RefSeq genes into three groups on the basis of their H3K27me2 and H3K27me1 levels. As shown in Figure 2C, H3K27me1 was preferentially enriched in the body of genes with high transcriptional activity, whereas H3K27me2 accumulated at genes with lower transcriptional rates. A similar result was observed for H3K27me2 and H3K36me3 (Figure 2C), whereas a positive correlation was seen between H3K27me1 and H3K36me3

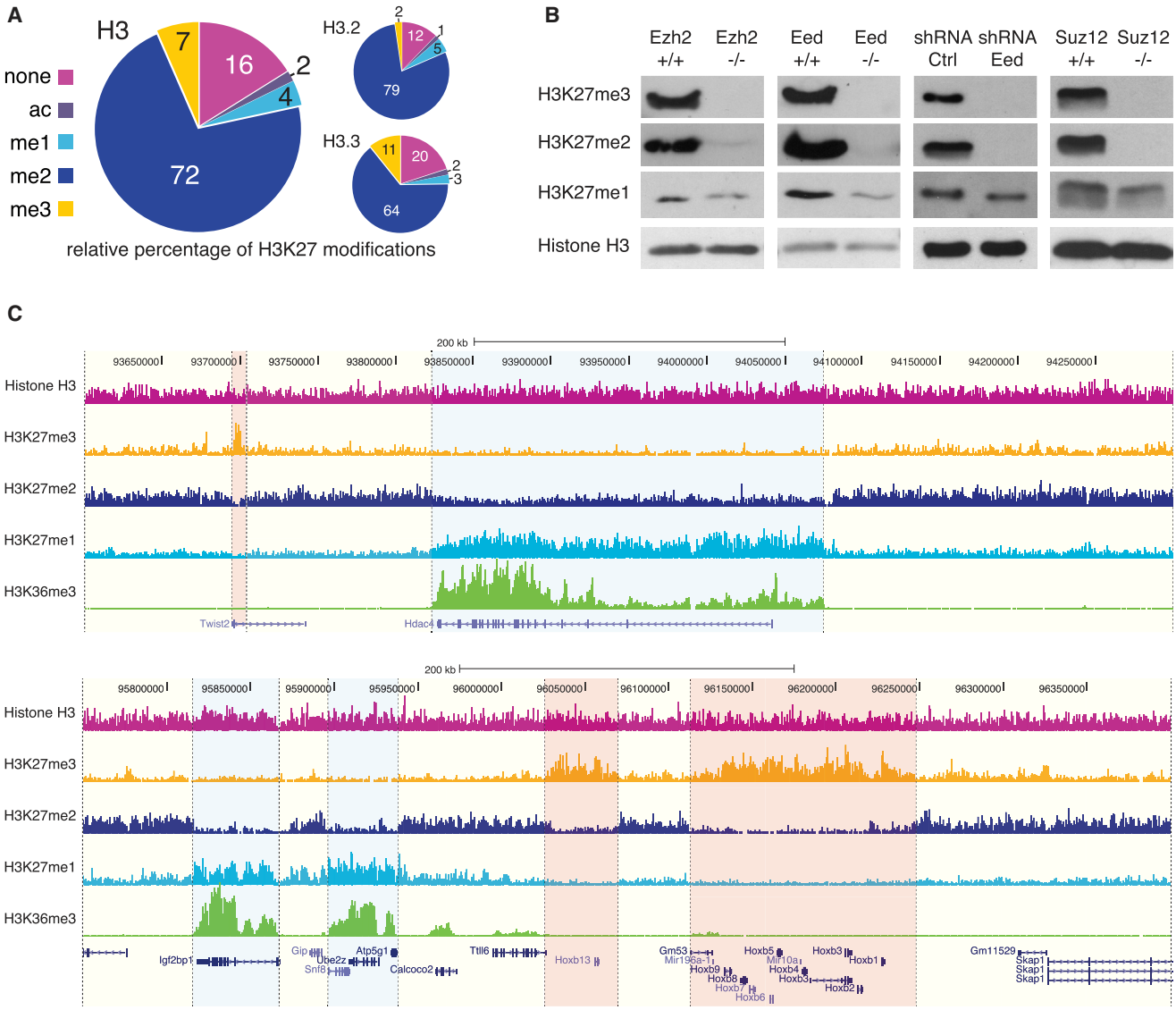

Figure 1. PRC2 Controls Distinct H3K27 Methylation Domains

(A) Relative abundance of H3K27 modifications in mouse ESCs by tandem MS analyses (Jung et al., 2010). The large pie represents the average abundance between histone H3.2 and H3.3 isoforms.

(B) Western blot analyses with the indicated antibodies of protein extracts obtained from WT (+/+) or *Eed*, *Ezh2*, or *Suz12* KO (−/−) mouse ESC lines or from mouse E14 ESCs stably infected with *Eed*-specific shRNAs. A scrambled shRNA sequence was used as a negative control (Ctrl). Histone H3 served as a loading control.

(C) Genomic snapshots of ChIP-seq experiments from E14 ESCs with the indicated antibodies. H3K27me1 domains are highlighted in blue, and H3K27me3 domains are highlighted in red.

See also Figures S1 and S2.

at the same intragenic sites (Figures 2A and 2B). Consistent with this, around 90% of all highly expressed genes were enriched in H3K27me1, whereas 90% of genes with low expression accumulated H3K27me2 throughout their gene bodies (Figures 2D, 2E, S3A, and S3B). Similar correlations were also obtained using RNA-seq data (Figure S3C). Overall, these data show that the different methylation forms of H3K27 define spatially distinct domains with different transcriptional properties.

H3K27me1 and H3K27me2 deposition did not correlate with a stable binding of the PRC2 complex. Given that members of the PRC2 complex were shown to localize at sites of ongoing replication (Hansen et al., 2008), we hypothesized that these modifications could be transiently deposited soon after the synthesis of newly replicated DNA strands. Western blot analyses on the pool of soluble respect to chromatin-associated histones confirmed that, in mouse ESCs, as previously reported for HeLa cells (Bonaldi et al., 2004; Garcia et al., 2007; Loyola

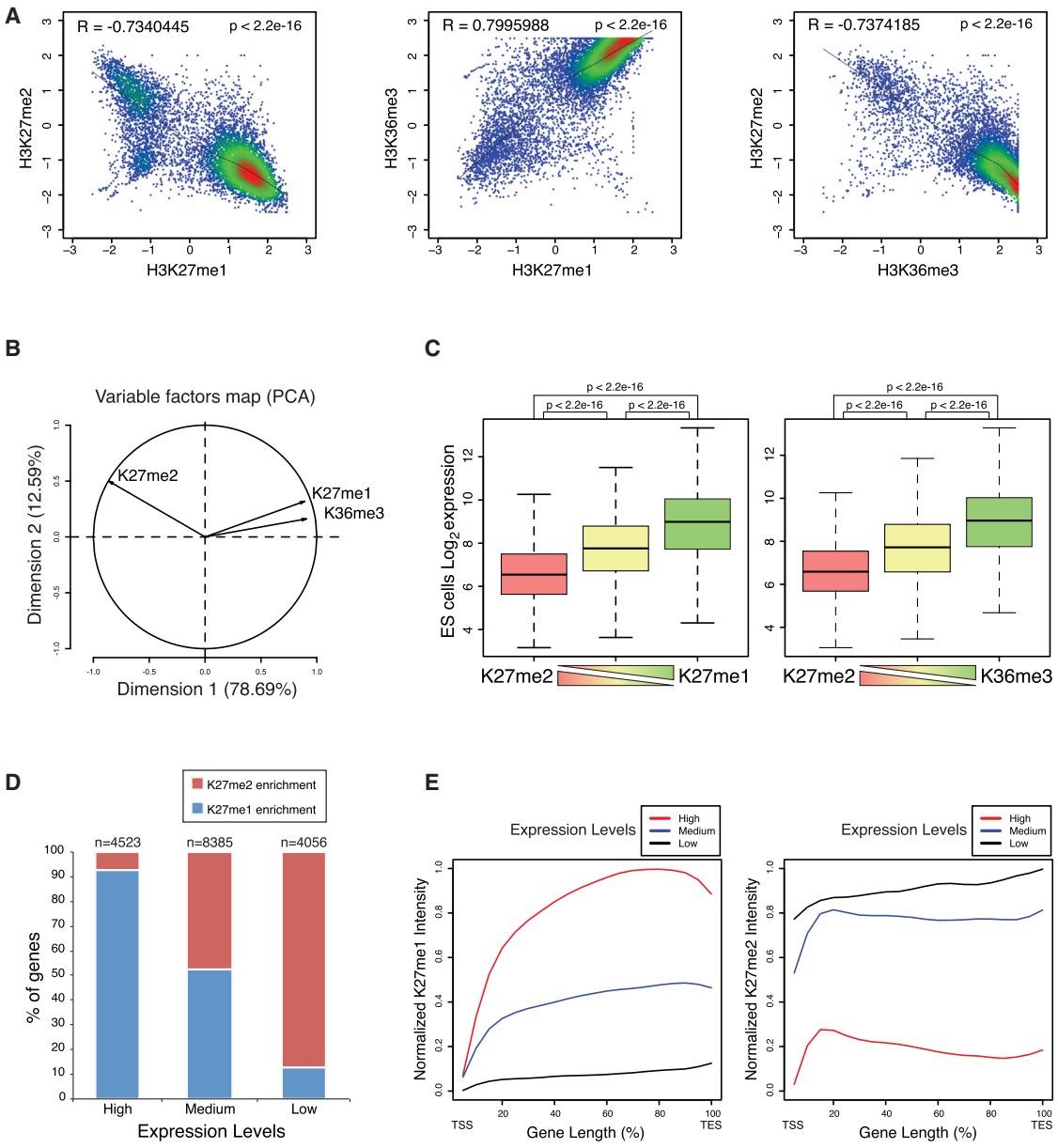

Figure 2. H3K27 Methylation Domains Show Mutually Exclusive Functional Correlations

(A) Plots showing the correlation between the enrichment normalized to the histone H3 density of the indicated PTMs within all RefSeq annotated genes. The R coefficient was determined with Pearson correlation. Left, n = 9,855; middle, n = 11,427; right, n = 9,358. p value was determined by student t test

(B) Biplot representing the degree of correlation between PTMs in gene bodies of all RefSeq annotated genes along first two dimensions. Correlation coefficients of K36me3, K27me1, and K27me2 with first the component are 0.9063163, 0.8917170, and −0.8626277.

(C) Expression levels from microarray analyses (Leeb et al., 2010) of all RefSeq genes (n = 19,895) divided in three equal groups after ranking for the relative abundance of H3K27me2 and H3K27me1 within gene bodies. p values were computed by a Student's t test.

(D) Gene counts depicting enrichments of H3K27me1 and H3K27me2 in each expression class. High expression, >third quantile; medium expression, <third quartile and >first quantile; low expression, <first quantile.

(E) Average profiles of H3K27me1 and H3K27me2 deposition along gene bodies (length expressed in percentages) for all three classes of gene sets shown in (D). See also Figure S3.

et al., 2006), H3K27 methylations were acquired after nucleosome assembly (Figure 3A). Thus, we tested the specificity of the H3K27me2 antibody in fluorescence-activated cell sorting (FACS) analyses using wild-type (WT) and *Eed* KO mouse ESCs (Figure 3B), pulsed growing mouse ESCs with BrdU in order to outline the S phase boundaries, and stained the cells with a H3K27me2-specific antibody to measure the accumulation of H3K27me2 throughout the different phases of the cell

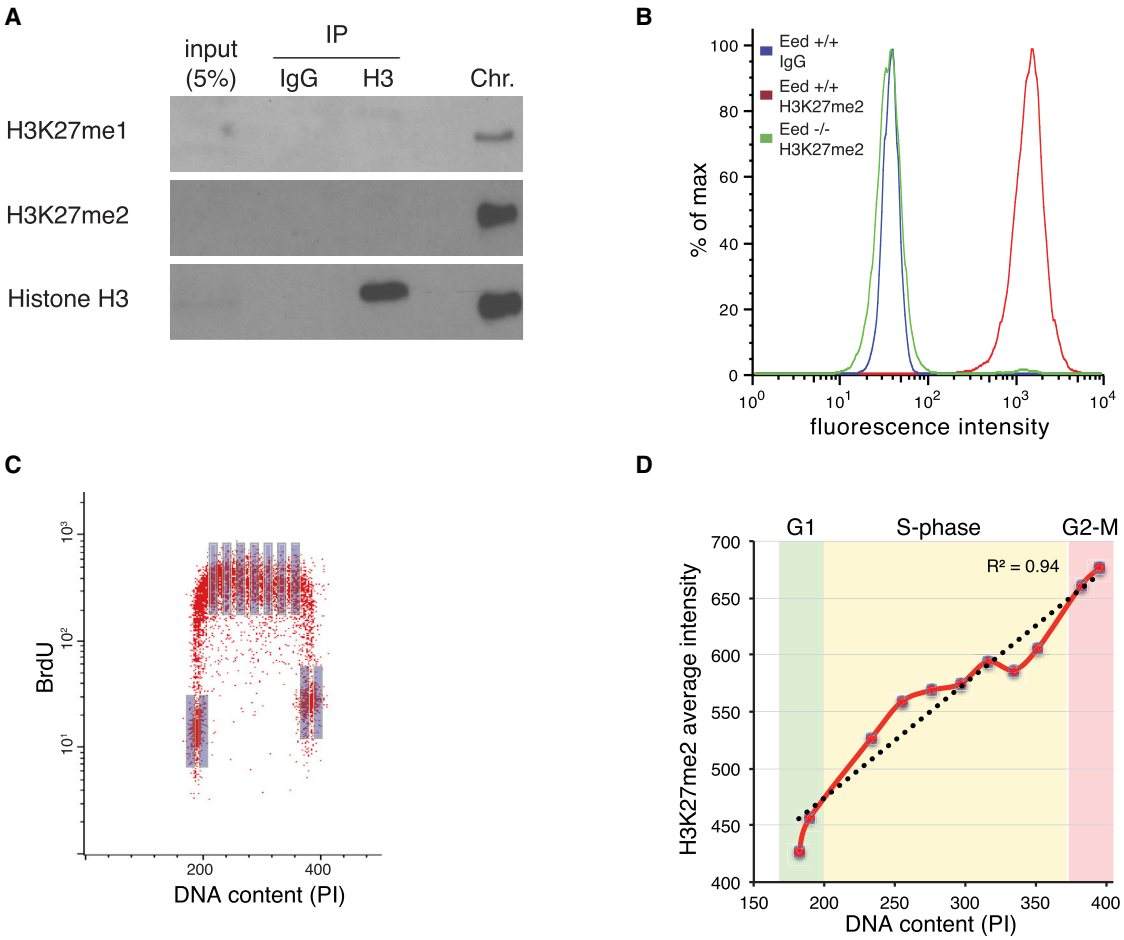

Figure 3. H3K27me2 Accumulates Linearly with the DNA Content during S Phase

(A) Western blots for H3K27me1 and H3K27me2 on immunopurified nonnucleosomal histone H3 from a soluble extract of E14 ESCs. Chromatin-bound histone H3 was used as positive control (Chr). Histone H3 served as loading control. Input was equal to 5% of total soluble extract.

(B) FACS analysis with H3K27me2 antibodies in WT (Eed +/+) and *Eed* KO (Eed −/−) mouse ESCs. Rabbit IgG served as a negative control.

(C) FACS analysis of BrdU and propidium iodide (PI) incorporation in WT mouse ESCs. Gray boxes indicate the gates used in (D).

(D) Correlation plot between the average fluorescence intensities of H3K27me2 and propidium iodide of the gates indicated in (C).

cycle (Figure 3C). The analysis showed that H3K27me2 accumulated linearly in S phase with respect to the increase of the DNA content depicted by propidium iodide, demonstrating a strong correlation (R^2 = 0.94) between DNA synthesis and H3K27me2 deposition (Figure 2D). Altogether, these data suggest that the PRC2 complex controls the modification of a large fraction of histone H3 during S phase progression.

PRC2 Deposits Intragenic H3K27me1 on a Genome-wide Level

To test whether intragenic H3K27me1 deposition was dependent on PRC2 activity, we performed ChIP analyses for H3K27me2 and H3K27me1 in WT and *Eed* KO mouse ESCs. Using real-time quantitative PCR (qPCR) primers placed inside or outside different genes that corresponded to areas of H3K27me1 and H3K27me2 accumulation, we demonstrated that intragenic H3K27me1 was lost in *Eed* KO cells (Figures 4A and S3D). Consistent with this, real-time qPCR ChIP analyses performed in *Suz12* and *Ezh2* KO mouse ESCs or in mouse ESCs expressing *Eed* shRNA further confirmed that the intragenic accumulation of H3K27me1 was dependent on the activity of the PRC2 complex (Figure 4B). Thus, to extend this observation at a genome-wide level, we performed H3K27me1 and H3K27me2 ChIP-seq analyses in WT and *Eed* KO mouse ESCs. The overlap between the H3K27me1 ChIP-seq analyses with E14 and *Eed* WT (E36) ESC lines highlighted the conservation of H3K27me1 deposition among different WT ESC lines (>90%; Figure S3E). The genomic snapshots presented in Figures 4C and S3F confirmed the real-time qPCR data and further demonstrated that H3K27me1 deposition was lost from additional genomic loci. Consistent with this, in *Eed* KO ESCs, H3K27me1 was lost from all the genes that were enriched for H3K27me1 in WT cells (Figures 4D and 4E). Overall, these data demonstrate that the intragenic accumulation of H3K27me1 in genes with a high transcriptional activity is dependent on the activity of the PRC2 complex.

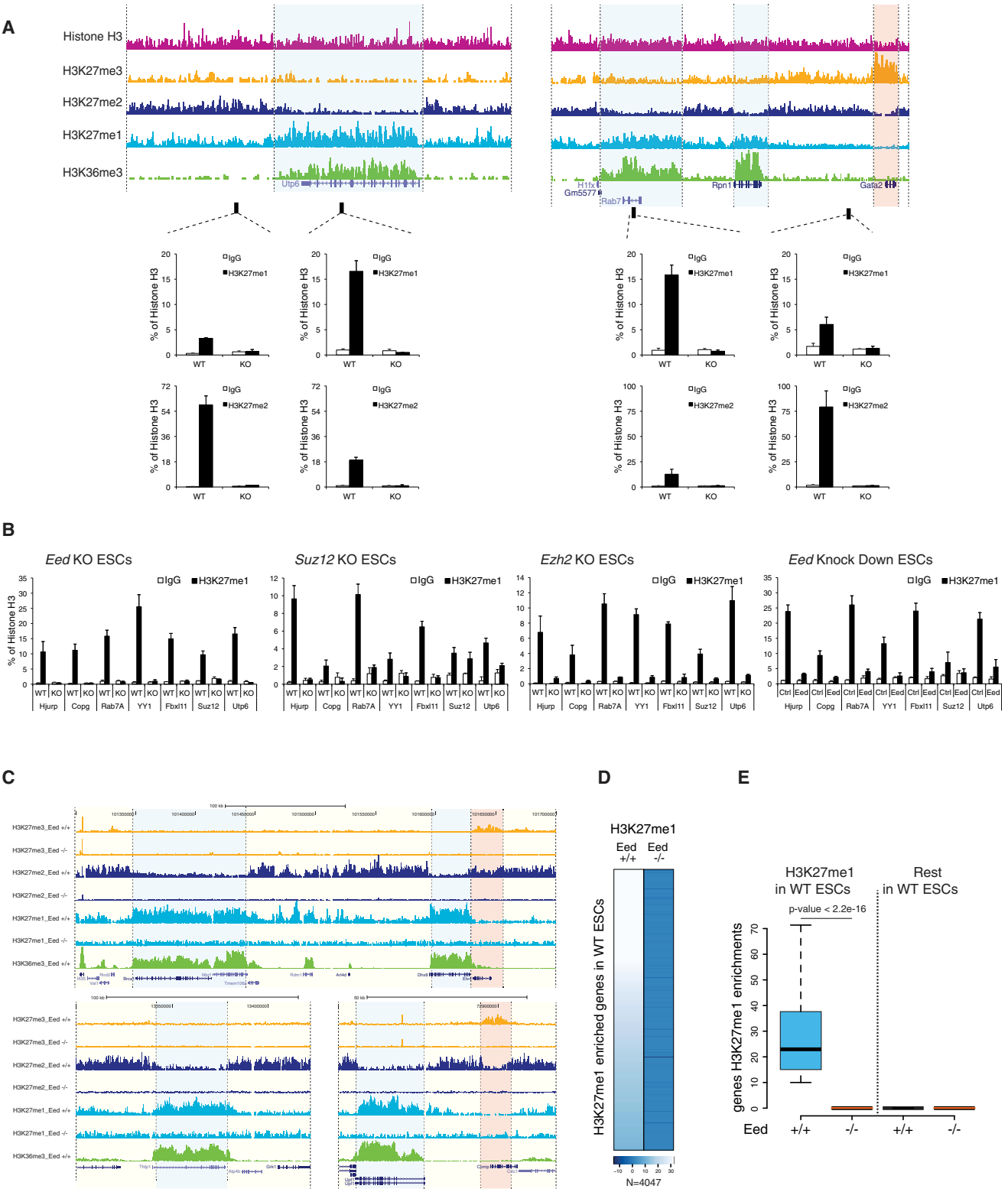

Figure 4. PRC2 Is Required for Genome-wide Intragenic H3K27me1 Deposition

(A) Real-time qPCR of ChIP analyses in WT and *Eed* KO ESCs using the indicated antibodies for the loci highlighted by the genomic snapshots. Black boxes indicate PCR amplicons. IgG rabbit served as a negative control. Enrichments are normalized to histone H3 density. Additional genomic loci are presented in Figure S3D. Data represent mean ± SEM.

(legend continued on next page)

PRC2-Dependent H3K27me1 Deposition Positively Correlates with Active Transcription

The correlation between the accumulation of different forms of H3K27 methylation and gene expression suggests that H3K27me1 deposition could play a positive role in promoting gene transcription. We took advantage of expression analyses performed in WT and *Eed* KO mouse ESCs (Leeb et al., 2010) to correlate the transcriptional changes of differentially expressed genes relatively to their intragenic H3K27 methylation state in WT ESCs. Remarkably, in *Eed* KO ESCs, the expression of genes enriched in H3K27me2 increased, whereas that of genes enriched in H3K27me1 decreased (Figure 5A). Both the expression and ChIP results were validated by independent real-time qPCR analyses (Figures 5B and 5C). Consistent with this, ChIP analyses in human embryonic kidney 293T cells expressing luciferase from an integrated heterologous promoter (Hansen et al., 2008) accumulated H3K27me1 within the luciferase coding sequence (Figure S4A). The repression of luciferase activity, mediated by forced recruitment of PRC2 to the heterologous promoter by the Gal4-Jarid2 fusion protein (Pasini et al., 2010), resulted in reduced H3K27me1 and H3K36me3 levels and an accumulation of H3K27me3 (Figure S4A). Overall, this result further confirmed the correlation between H3K27me1 with active transcription and suggests that the stable recruitment of the PRC2 complex to DNA induces the full conversion of H3K27 to its trimethylated form.

To gain additional insight about the relationship between H3K27me1 and gene transcriptional regulation, we induced WT and *Eed* KO mouse ESCs to differentiate in cell culture through the formation of embryoid bodies (EBs). Consistent with previous reports (Schoeftner et al., 2006), the loss of *Eed* impaired proper mouse ESC differentiation, as depicted by the lack of activation of EB differentiation markers (Figure S4B). ChIP analyses for H3K27me1 and H3K36me3 within the body of genes that failed to undergo transcriptional activation in *Eed* KO EBs showed that, although the accumulation of H3K36me3 was moderately affected, H3K27me1 deposition was fully dependent on PRC2 activity (Figure 5D). RNA-seq analyses on WT and *Eed* KO EBs confirmed this result, showing that global gene activation was significantly reduced in *Eed* KO EBs and that this correlated with the lack of H3K27me1 deposition without globally affecting H3K36me3 levels (Figures 5E, 5F, and S4C). Altogether, these data demonstrate that H3K27me1 deposition is still dependent on PRC2 activity in differentiating ESCs and suggest that H3K36me3 could function upstream of H3K27me1 deposition.

H3K27me1 Deposition Is Controlled by Setd2-Dependent H3K36 Trimethylation

To test whether the accumulation of H3K27me1 could be influenced by H3K36me3 deposition, we knocked down the expression of different H3K36 KMTs (data not shown). This identified Setd2 as the main enzyme that regulates H3K36me3 levels in mouse ESCs (Figure 6A). ChIP analyses of mouse ESCs that expressed control or *Setd2*-specific shRNAs revealed that the loss of H3K36me3 (Figure 6A) correlated with reduced intragenic H3K27me1 levels as well as the accumulation of H3K27me2 (Figure 6B). Consistent with this, the acute loss of Setd2 expression reduced the transcription of a significant number of genes that were previously found repressed in *Eed* KO ESCs (Figure S5A). The loss of Setd2 expression did not alter the overall expression levels of different PRC2 components (data not shown), nor did it affect PRC2 colocalization with DNA replication foci in S phase cells (Figure S5B). These results suggest that H3K36me3 deposition can regulate the formation of H3K27me1 domains by inhibiting PRC2-dependent H3K27me2 conversion. This hypothesis is in agreement with previous analyses showing that H3K36me3 inhibits the in vitro deposition of H3K27me2 and H3K27me3 but still allows the efficient formation of H3K27me1 on nucleosomal substrates (Schmitges et al., 2011; Yuan et al., 2011). This is consistent with the inability of PRC2 activity in vitro for generating H3K27me2 in the presence of a fully H3K36me3-modified histone H3 (Figure S5C). Mass spectrometry data on H3K36me3 purified histones demonstrated that H3K27me1 and H3K36me3 modifications coexist on the same histone tail (Figures S5D–S5F), a result that supports a *cis*-acting mechanism for the regulation of H3K27me1 accumulation. This double modification was detected only in the histone variant H3.3 (Figures S5E and S5F), which is also consistent with the preferential H3.3 accumulation within the intragenic regions of highly expressed genes (Goldberg et al., 2010). Overall, these data suggest that the deposition of H3K36me3 regulates PRC2 activity by inhibiting the conversion of H3K27me1 to H3K27me2.

H3K27me2 Prevents Firing of Non-Cell-Type-Specific Enhancers

In contrast to H3K27me1, H3K27me2 is broadly distributed throughout the genome and deposited at approximately 70% of all the histone H3 present in ESCs (Figures 1A and 1C). Although it is possible that this H3K27me2 deposition merely "fills the gaps" between functionally defined regions marked by H3K27me1 and H3K27me3, H3K27me2 could also have

(B) Real-time qPCR of ChIP analysis in the specified mouse ESC lines for the indicated intragenic regions with the specified antibodies. IgG rabbit served as a negative control. Enrichments are normalized to histone H3 density. Data represent mean ± SEM.
(C) Genomic snapshots of H3K27me1, H3K27me2, and H3K27me3 ChIP-seq analyses in WT (Eed +/+) and *Eed* KO (Eed −/−) ESCs along with H3K36me3 ChIP-seq analyses from E14 ESCs. H3K27me1 domains are highlighted in blue, and H3K27me3 domains are highlighted in red. Additional genomic loci are presented in Figure S3F.
(D) Heat map of the normalized H3K27me1 ChIP-seq signal in WT (Eed +/+) and *Eed* KO (Eed −/−) mouse ESCs for H3K27me1-enriched genes in WT mouse ESCs (−10log p value ≥ 10 of a chi-square test between H3K27me1 and H3).
(E) Box plots of H3K27me1 ChIP-seq intensities between WT (+/+) and *Eed* KO (−/−) ESCs as in (D) of RefSeq genes divided in two groups on the basis of H3K27me1 enrichments in WT cells (−10log p value cutoff = 10). H3K27me1-positive genes, n = 4,047; rest of genes, n = 22,466. p value was calculated by a Student's t test.
See also Figures S2 and S3.

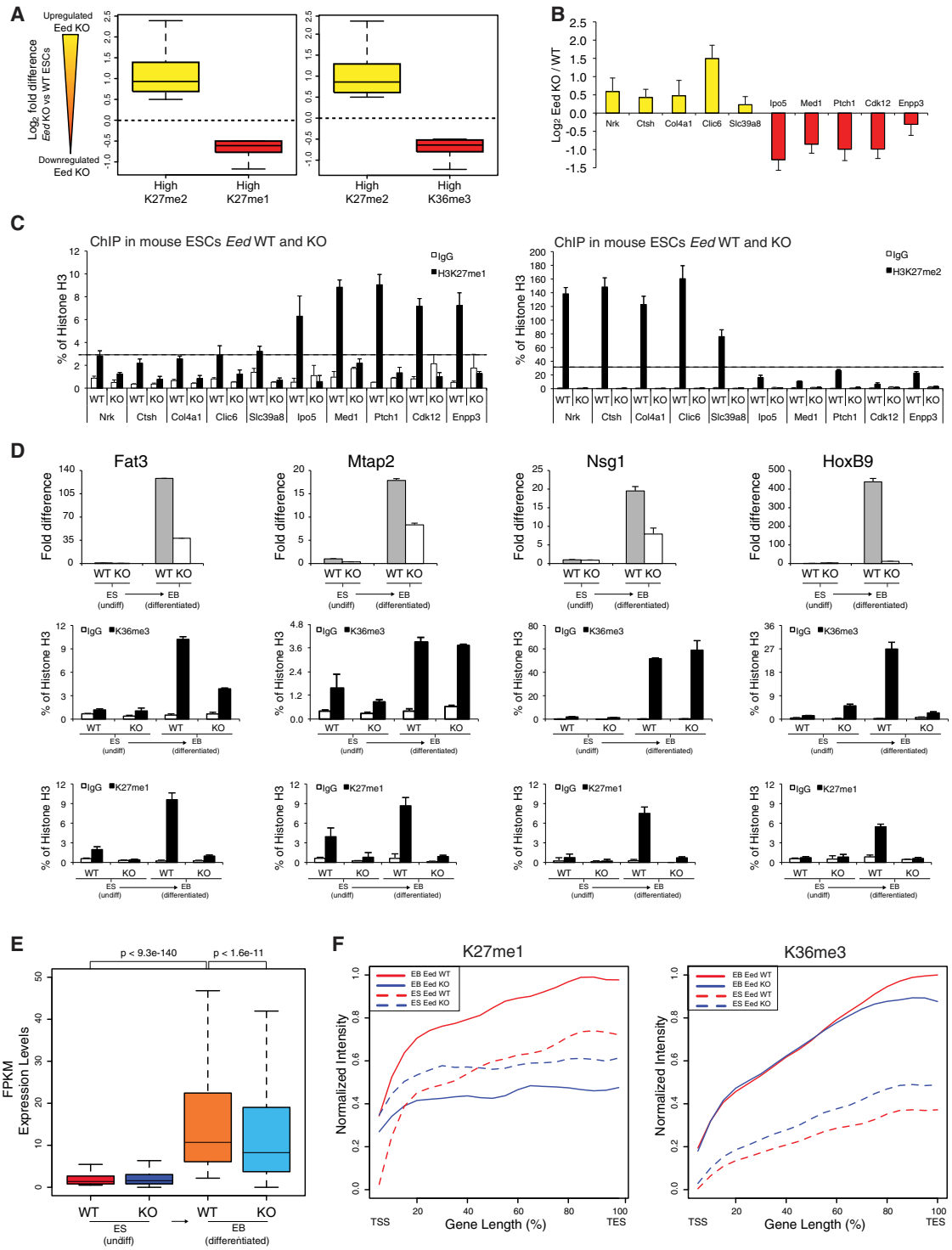

Figure 5. PRC2-Dependent H3K27me1 Deposition Is Required for Correct Transcription

(A) Box plot of the expression changes of differentially regulated genes between WT and *Eed* KO mouse ESCs for the H3K27me2 and H3K27me1 top 10% enriched genes (n = 2,647).

(B) Relative expression differences between WT and *Eed* KO mouse ESCs of the indicated genes determined by real-time qPCR analysis. Gene expression is normalized to Gapdh levels. Data represent mean ± SEM.

(C) Real-time qPCR ChIP analyses with primers for the indicated intragenic regions in WT and *Eed* KO ESCs with the indicated antibodies. IgG rabbit served as a negative control. Enrichments are normalized to histone H3 density. Data represent mean ± SEM.

(legend continued on next page)

specific functions in genomic control and organization. Consistent with previous reports (Pasini et al., 2010; Tie et al., 2009), the loss of PRC2 activity globally increased the levels of H3K27Ac (Figure 7A). Interestingly, H3K27ac was recently characterized as a histone PTM that distinguishes between active and poised enhancer elements (Creyghton et al., 2010; Rada-Iglesias et al., 2011). At transcription start sites (TSSs), H3K27ac accumulates in the presence of H3K4me3, whereas, at regulatory enhancer elements, H3K27ac is found in combination with H3K4me1, thus determining their active versus poised state (Creyghton et al., 2010; Heintzman et al., 2007; Rada-Iglesias et al., 2011). To characterize the genome-wide distribution of H3K27ac induced by the loss of PRC2 activity, we performed ChIP-seq analyses for H3K27ac in WT and *Eed* KO mouse ESCs. This revealed that H3K27ac was differentially accumulated in WT and KO cells; whereas some peaks were only present in WT cells (Eed WT unique, Figures 7B, 7C, S6A, and S6B), several H3K27ac peaks were specifically acquired in *Eed* KO cells (Eed KO unique, Figures 7B, 7C, S6A, and S6B). The annotation of these peaks, relative to a ±2.5 kb region across RefSeq TSSs, showed that common peaks between WT and *Eed* KO mouse ESCs were almost equally distributed between TSS and non-TSS regions (Figure 7B). Instead, the differentially regulated H3K27ac peaks between WT and *Eed* KO mouse ESCs were preferentially found at sites that did not overlap with gene TSSs (Figure 7B). Given that the global difference in H3K27ac levels between the two samples could introduce biases into the ChIP-seq analyses, we further confirmed these results with independent real-time qPCR ChIP analyses, validating both the loss and gain of H3K27ac (Figure S6A).

Altogether, these results suggest that PRC2 activity can induce changes in H3K27ac at potential regulatory elements, implying that the broad H3K27me2 deposition could exert protective functions by preventing the activation of non-cell-type specific enhancer elements. Thus, we extended our ChIP-seq analyses to H3K4me1 and H3K4me3 in order to map enhancer elements in both WT and *Eed* KO mouse ESCs. Genomic snapshots of these analyses showed that new sites of H3K27ac deposition are enriched for H3K4me1 but lack H3K4me3 (Figures 7C, 7E, S6B, and S6C). This result was further confirmed when the entire set of Eed WT and KO unique enhancers was analyzed, highlighting the existence of two classes of activated enhancers in *Eed* KO cells (Figures 7D and 7E). A first class was premarked by H3K4me1 (class I), and a second class was not monomethylated on H3K4 in WT ESCs and accumulated H3K4me1 in correlation with H3K27ac deposition (class II). Although in the absence of PRC2 activity H3K27ac was preferentially deposited at sites that were premarked with H3K4me1 (~60%), this result showed that H3K27ac could also accumulate on sites that did not contain H3K4me1, inducing its subsequent deposition (~40%) (Figures 7D and 7E). Importantly, for both classes of Eed KO enhancers, the lack of H3K27ac correlated with increased levels of H3K27me2 (Figures 7D and 7E). In addition, the negative correlation observed between the deposition of H3K27ac and H3K27me2 in WT ESCs at unique enhancer sites (Figure 7F) further supports the protective role of H3K27me2. These regulatory elements differ from the H3K27me3-enriched enhancers previously described in human ESCs (Creyghton et al., 2010; Rada-Iglesias et al., 2011) and represent a larger set of poised enhancers in ESCs. Indeed, the large majority of poised enhancers (defined by high-H3K4me1 and low-H3K4me3 levels and no H3K27ac) retained low H3K27me3 levels in both human and mouse ESCs (Figure S7A). Consistent with this, the same sites did not show any significant Ezh2 association when compared to CpG-rich genomic elements, known targets of PRC2 binding and H3K27me3 deposition (Figures S7B and S7C).

Importantly, the genes found in close proximity to Eed KO unique enhancers were preferentially upregulated in the absence of Eed expression (Figure S7D). Consistent with this, the relative distance to the closest activated gene was significantly reduced for the enhancers that acquired H3K27ac in Eed KO ESCs regardless of H3K27me3 deposition at their promoters in WT ESCs (Figure S7E). Our model implies that H3K27me2 is globally distributed along the genome in order to prevent a deregulated positioning of H3K27ac. This model also implies that the loss of H3K27ac should be rapidly protected by the deposition of H3K27me2. To test this possibility, we inhibited p300 and Cbp activity in WT ESCs with the histone acetyltransferase (HAT) inhibitor C646 (Figure S7F) and identified more than 4,800 enhancer sites that had lost H3K27ac upon treatment (Figures 7G and S7F). Consistent with our hypothesis, the loss of H3K27ac from these sites led to them being "filled" by the deposition of H3K27me2 (Figure 7G). This result demonstrates that the loss of H3K27ac from regulatory elements is rapidly occupied by H3K27me2 deposition and further supports a protective role for the broad distribution of this modification.

DISCUSSION

Different studies have shown that the loss of PRC2 activity induces the deregulation of the expression of several genes, of which only a small fraction (~5%–10%) is directly targeted by H3K27me3 to their promoters (Boyer et al., 2006; Bracken et al., 2006; Lee et al., 2006). This observation suggests that the deregulation of a set of genes induces phenotypic effects

(D) Top, relative expression of the indicated genes determined by qRT-PCR in WT and *Eed* KO ESCs before (ES) and after (EB) differentiation. Gene expression is normalized to *Gapdh* levels. Middle and bottom, real-time qPCR ChIP analyses in the same cells with primers for the indicated intragenic regions with the indicated antibodies. IgG rabbit served as a negative control. Enrichments are normalized to histone H3 density. Data represent mean ± SEM.
(E) Expression levels of genes upregulated (≥4-fold) during differentiation in WT and *Eed* KO samples (N = 844). The p values were determined by a Wilcoxon rank test.
(F) Average profiles of H3K27me1 and H3K36me3 deposition along the gene body (length expressed in percentages) for genes activated upon EB differentiation shown in (E), n = 844.
See also Figure S4.

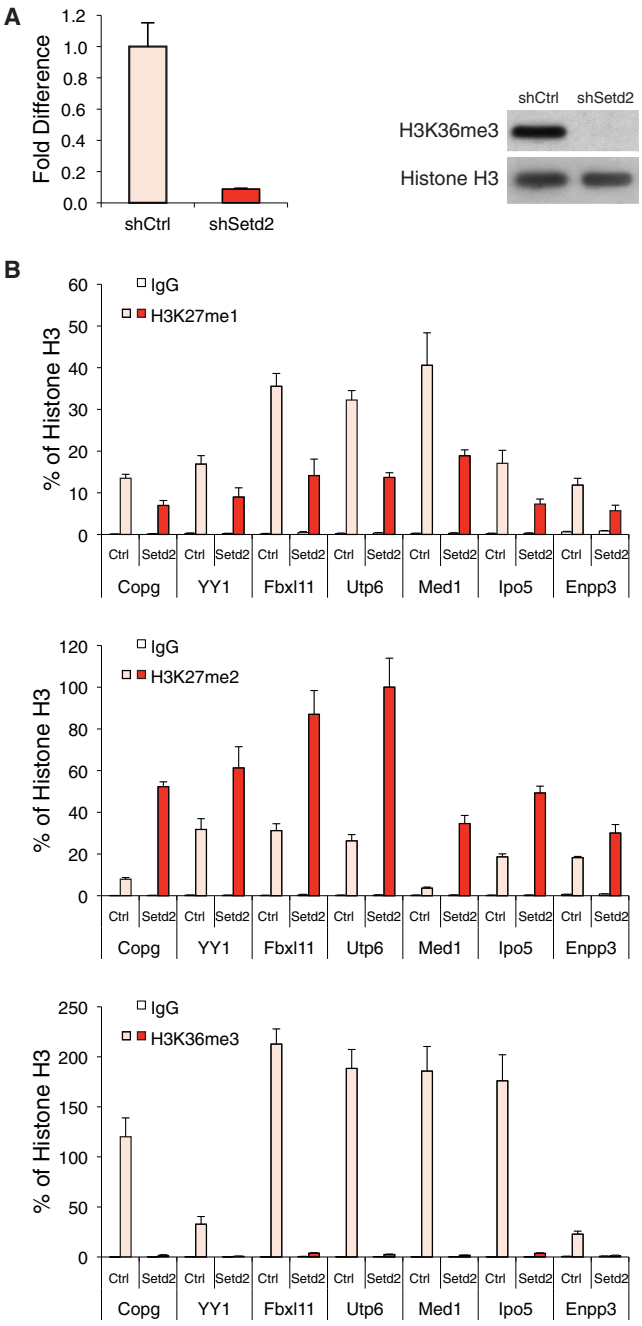

Figure 6. Setd2-Dependent H3K36me3 Controls PRC2 Enzymatic Activity In Vivo

(A) Expression levels of *Setd2* by real-time qPCR analyses in cells expressing scrambled (shCtrl) or *Setd2*-specific shRNAs (shSetd2). Gene expression is normalized to *Gapdh* levels. Western blot analysis with H3K36me3 specific antibody on protein extracts from the same cells. Histone H3 was used as a loading control. Data represent mean ± SEM.

(B) Real-time qPCR ChIP analyses in the same cells presented in (A) with primers for the indicated intragenic regions with the indicated antibodies. Rabbit IgG served as a negative control. Enrichments are normalized to histone H3 density. Data represent mean ± SEM.

See also Figure S5.

that reflect in broader transcriptional changes. Our results provide additional explanations for PRC2-mediated transcriptional deregulation, suggesting that both H3K27me1 and H3K27me2 can directly influence gene expression to control active transcription and enhancer fidelity, respectively.

PRC2 Controls the Modification of the Majority of Histone H3K27 in Mouse ESCs

The PRC2 complex controls the H3K27 methylation of nearly the entire bulk of histone H3 (~80%) present in mouse ESCs, which is in agreement with previous mass spectrometry (MS) studies (Schoeftner et al., 2006). Our ChIP-seq data confirm and extend this observation, showing how different methylated states of H3K27 form mutually exclusive genomic domains. The diffused H3K27me2 signal is consistent with the MS quantifications and demonstrates that PRC2 has a general activity in modifying large regions of chromatin. In addition, the finding that H3K27me1 preferentially accumulates within the body of highly expressed genes is consistent with previous reports that characterized the epigenome of human $CD4^+$ T cells, suggesting that this activity is not only restricted to mouse ESCs (Barski et al., 2007).

Histone H3K27 Methylation Occurs in the Absence of Stable PRC2 Binding

Our data also demonstrate that the large majority of PRC2 KMT activity occurs at chromatin sites where PRC2 is not stably associated. Previous in vitro studies showed that PRC2 efficiently methylates H3K27me0 and H3K27me1 but modifies H3K27me2 substrates with reduced efficiency (McCabe et al., 2012). Hence, although the deposition of H3K27me1 and H3K27me2 may take place through a transient interaction of PRC2 with the nucleosomes, efficient conversion to H3K27me3 could require a stable binding of PRC2 at specific sites. Given that more than 70% of histone H3 is dimethylated on H3K27, we propose that H3K27me2 is the main activity of the PRC2 complex and that additional mechanisms control PRC2 enzymatic activity in order to determine H3K27me1 and H3K27me3 accumulation at specific genomic loci.

We have previously reported that PRC2 can localize at the foci of ongoing DNA replication in order to conserve H3K27me3 in the newly incorporated histones (Hansen et al., 2008). However, H3K27me3 is present in mouse ESCs in approximately 7,000 discrete peaks (Mikkelsen et al., 2007), and, considering that about 90% of BrdU foci were found in overlap with the Ezh2 staining (Hansen et al., 2008), it is unrealistic that such localization merely involves H3K27me3 deposition. It is possible that association with ongoing replication is not coupled to H3K27me3 deposition but rather to the broader H3K27me2 distribution (and, to a lesser extent, that of H3K27me1), which would explain the large PRC2 localization at replication sites. The linear deposition of H3K27me2 along with DNA synthesis is consistent with this assumption and suggests a model in which H3K27me2 and H3K27me1 deposition is coupled to DNA synthesis, whereas, in contrast, H3K27me3 accumulation is a slower event that takes place through specific association of PRC2 with CpG-rich elements. This model is in agreement with other reports showing that, after DNA synthesis,

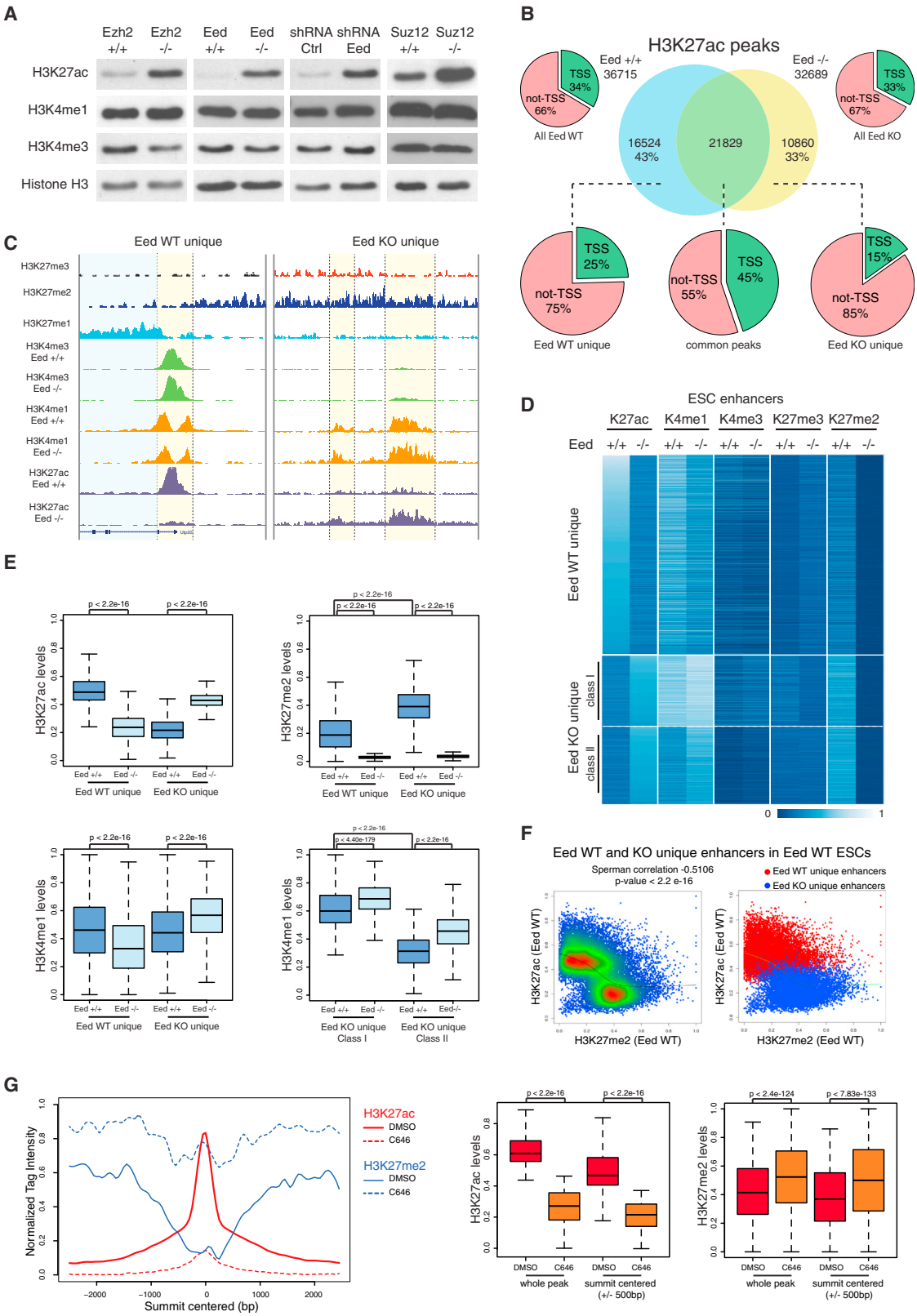

(legend on next page)

H3K27me1 and H3K27me2 are rapidly incorporated, but the restoration of normal H3K27me3 levels is delayed (Lanzuolo et al., 2011; Scharf et al., 2009). This model is also in agreement with the accumulation of H3K27me3 observed upon forced recruitment of PRC2 to a heterologous promoter. The lack of H3K27 modification in the soluble histone pool implies that all H3K27 methylations occur after nucleosome assembly. It's possible that yet unidentified components link PRC2 activity to the replication sites. Alternatively, PRC2 subunits with histone binding proprieties, such as Rbbp4 and Rbbp7 or the PHD-containing proteins Phf1, Mtf2, and Phf19, could rapidly sense the methylation state of newly assembled nucleosomes.

H3K36me3 Regulates the Formation of H3K27me1 and H3K27me2 Domains

Our results also suggest that the presence of H3K36me3 controls the ratio between PRC2-dependent H3K27me2 and H3K27me1 deposition. This model is supported by the coexistence of H3K36me3 and H3K27me1 on the same histone tail as well as by the reduced efficiency of the PRC2 complex in accumulating H3K27me2 when histone H3 tails are modified with K36me3 (Schmitges et al., 2011) (Figure S5C). Altogether, these evidences support a model wherein the PRC2 complex catalyzes a broad H3K27me2 deposition soon after the DNA is synthesized. It forms H3K27me1 domains on actively transcribed genes via Setd2-dependent H3K36me3 deposition and accumulates H3K27me3 only upon stable binding to CpG-rich DNA loci.

Regulation of Transcription by H3K27me1 and H3K36me3 Deposition

The strong relationship between H3K36me3 and the decreased expression of H3K27me1-positive genes in *Eed* KO mouse ESCs suggests that PRC2 activity could have a positive role in regulating gene expression. H3K36me3 deposition is regulated by RNAPII Ser2 phosphorylation, determining Setd2 recruitment and H3K36me3 accumulation at transcribed genes (Phatnani and Greenleaf, 2006). The deposition of H3K27me1 along with H3K36me3 may be linked with the higher mobility of histones and nucleosomes required at sites of transcriptional elongation. Alternatively, H3K27me1 could play a role in connecting H3K36me3 with pre-mRNA splicing (de Almeida et al., 2011).

Loss of H3K27me2 Disrupts Canonical ESC-Specific Enhancer Regulation

The global increase of H3K27ac in PRC2-deficient mouse ESCs suggests that the loss of PRC2 activity renders chromatin accessible for HAT activity. Our data show that, although promoter acetylation is less affected, the loss of PRC2 activity induces profound changes in H3K27 acetylation at enhancer elements. Although the mechanisms of enhancer specification, activation, and target regulation are still poorly understood, it is known that enhancers can be found in either a poised or an active state (Jin et al., 2011; Ong and Corces, 2011). Although the accumulation of H3K4me1 and low levels of H3K4me3 characterize both poised and active enhancers, H3K27 acetylation distinguishes their active from poised states. We show that, along with a general increase of H3K27ac levels, the loss of PRC2 activity induces the activation of poised enhancers in mouse ESCs. It is possible that the broad "unspecific" deposition of H3K27me2 protects H3K27 from HAT activity and that global loss of H3K27me2 creates HAT accessibility inducing noncanonical enhancer firing. This allows speculation that the broad "unspecific" deposition of H3K27me2 protects H3K27 from HAT activity. This is supported by the rapid deposition of H3K27me2 at sites that lose H3K27ac upon the inhibition of HAT activity. However, this result opens also to the possibility that the deposition of H3K27ac function in preventing the spreading of H3K27me2 at active sites. Furthermore, the fact that H3K27ac preferentially accumulates in the presence of H3K4me1 suggests a direct link between HAT recruitment and H3K4me1; however, this mechanism is not exclusive, and a large fraction of activated enhancers (40%) accumulated H3K4me1 as a consequence of H3K27ac deposition. Although the global increase of H3K27ac might have additional functions, the relationship between the activated enhancers and gene transcriptional reactivation suggests that the aberrant activation of noncanonical enhancers could

Figure 7. Loss of H3K27me2 Disrupts Canonical ESC-Specific Enhancer Regulation

(A) Western blots with the indicated antibodies of protein extracts from WT (+/+) and *Eed*, *Ezh2*, or *Suz12* KO (−/−) ESCs or from E14 ESCs expressing scrambled (Ctrl) and *Eed*-specific shRNAs. Histone H3 served as loading control.

(B) Genome-wide overlap of H3K27ac peaks between WT and *Eed* KO mouse ESCs. The pies represent the distribution of H3K27ac peaks relative to RefSeq promoter regions defined as a 5 kb region centered on the TSS.

(C) Genomic snapshots of ChIP-seq analyses for H3K27me1, H3K27me2, H3K27me3, H3K27ac, H3K4me1, and H3K4me3 in WT (Eed +/+) and *Eed* KO (Eed −/−) mouse ESCs. Regions of regulated H3K27ac are highlighted in yellow. Additional snapshots of the same analysis are presented in Figure S6B.

(D) Heat map of the indicated normalized intensities in WT (+/+) and *Eed* KO (−/−) ESCs at H3K27ac distal peaks unique in WT (Eed WT unique peaks, n = 12,341) or *Eed* KO (Eed KO unique peaks, n = 9,210) shown in (B). Eed KO unique peaks were divided into class I (n = 4,391) and class II (n = 4,819) groups by k mean clustering (k = 2) with respect to the H3K4me1 normalized intensities in Eed WT ESCs.

(E) Box plots quantifying the data shown in (D). Additional analyses for H3K4me3 and H3K27me3 are presented in Figure S6C. Eed WT unique peaks, n = 12,341; Eed KO unique peaks, n = 9,210. p value was calculated by a Wilcoxon rank test.

(F) Scatter plot correlation of the H3K27ac versus H3K27me2 levels in WT ESCs for unique enhancers identified in WT and Eed KO ESCs. Left, whole density distributions. Right, the modification levels of Eed WT unique (red) and Eed KO unique (blue) enhancers. The Spearman correlation value is indicated ($r_s = -0.5106$). p value was calculated by asymptotic t approximation.

(G) Average profiles of H3K27ac and H3K27me2 deposition across a genomic window of ± 2,500 bp (centered to the H3K27ac peak summit) for active enhancers that lose H3K27ac deposition upon treatment with 35 μM C646 compound for 48 hr (n = 4,838). DMSO was used as a vehicle control. The box plots on the right show the quantification of the H3K27ac and H3K27me2 levels at the same enhancer sites upon treatment with C646 for the whole H3K27ac peak region or for a 1 kb genomic region surrounding the summit of each H3K27ac peak. p value was calculated by a Wilcoxon rank test.

See also Figures S6 and S7.

contribute to the developmental and lineage specification defects observed in the absence of PRC2 activity. Overall, we propose that, although H3K27me3 accumulation is involved in the cell-type-specific maintenance of gene transcriptional repression (Mohn et al., 2008), the depositions of H3K27me2 and H3K27me1 have structural and protective functions that are transversally conserved among cell types, thus identifying mechanisms by which PRC2 activity can regulate transcription and cell-fate decisions.

EXPERIMENTAL PROCEDURES

Tissue Culture and Cell Manipulation

All ESCs were grown on feeder-free medium in the presence of leukemia inhibitory factor. Ebs differentiation was achieved by hanging drop formation in presence of all-*trans* retinoic acid. Knockdown experiments were performed either with shRNAs or endoribonuclease-prepared siRNAs, as indicated in the figures and their corresponding legends. Detailed protocols of cell culture and manipulation are available in the the Supplemental Information.

Antibodies

A detailed list of antibodies is available in the Supplemental Information.

Cell-Cycle Analysis and Flow Cytometry

E14 ESCs were pulsed with 33 μM BrdU for 15 min, ethanol fixed, and stained with anti H3K27me2 (Cell Signaling, 9728), BrdU (BD Biosciences), and propidium iodide. A detailed protocol of staining and FACS acquisition is available in the Supplemental Information.

ChIP- and RNA-Sequencing

ChIP assays were carried out as described previously (Pasini et al., 2010), and DNA libraries were prepared with an Illumina TruSeq kit. RNA was extracted with TRIzol Reagent (Invitrogen, 15596) and converted to double-stranded complimentary DNA with the TruSeq kit. Samples were deep sequenced with an Illumina HiSeq 2000 system. Detailed protocols are available in the Supplemental Information.

Sequencing and Expression Data Analysis

Detailed descriptions of data processing and all bioinformatic analyses are available in the Supplemental Information.

Real-Time qPCR and Primers

Real-time qPCR analyses were carried out as described previously (Pasini et al., 2008). Primer sequences are available in Table S5, and additional information is provided in the Supplemental Information.

ACCESSION NUMBERS

Raw ChIP- and RNA-seq data have been deposited in the NCBI Gene Expression Omnibus under accession numbers GSE39496 and GSE51006.

SUPPLEMENTAL INFORMATION

Supplemental Information contains Supplemental Experimental Procedures, seven figures, and two tables and can be found with this article online at http://dx.doi.org/10.1016/j.molcel.2013.10.030.

ACKNOWLEDGMENTS

We thank all members of the Pasini laboratory for helpful discussion; Hye Ryung Jung and Ole Nørregaard Jensen for MS data support; Gabriele Bucci, Davide Cittaro, Gioacchino Natoli, and Saverio Minucci for general support; Andrea Piunti for his comments; Anton Wutz for the mouse *Eed* KO ESCs; and Veronica Raker for help editing the manuscript. D.P. was supported by the Italian Association for Cancer Research and by the Italian Ministry of Health. T.B. was supported by grants from the Giovanni Armenise-Harvard Foundation Career Development Program, the Association of International Cancer Research, the Italian Association for Cancer Research, and the Cariplo Foundation. I.B. was supported by a fellowship of the Italian Cancer Research Foundation.

Received: July 25, 2013
Revised: September 23, 2013
Accepted: October 24, 2013
Published: November 27, 2013

REFERENCES

Aloia, L., Di Stefano, B., and Di Croce, L. (2013). Polycomb complexes in stem cells and embryonic development. Development *140*, 2525–2534.

Barski, A., Cuddapah, S., Cui, K., Roh, T.Y., Schones, D.E., Wang, Z., Wei, G., Chepelev, I., and Zhao, K. (2007). High-resolution profiling of histone methylations in the human genome. Cell *129*, 823–837.

Berger, S.L. (2007). The complex language of chromatin regulation during transcription. Nature *447*, 407–412.

Bonaldi, T., Regula, J.T., and Imhof, A. (2004). The use of mass spectrometry for the analysis of histone modifications. Methods Enzymol. *377*, 111–130.

Boyer, L.A., Plath, K., Zeitlinger, J., Brambrink, T., Medeiros, L.A., Lee, T.I., Levine, S.S., Wernig, M., Tajonar, A., Ray, M.K., et al. (2006). Polycomb complexes repress developmental regulators in murine embryonic stem cells. Nature *441*, 349–353.

Bracken, A.P., and Helin, K. (2009). Polycomb group proteins: navigators of lineage pathways led astray in cancer. Nat. Rev. Cancer *9*, 773–784.

Bracken, A.P., Dietrich, N., Pasini, D., Hansen, K.H., and Helin, K. (2006). Genome-wide mapping of Polycomb target genes unravels their roles in cell fate transitions. Genes Dev. *20*, 1123–1136.

Cao, R., and Zhang, Y. (2004). SUZ12 is required for both the histone methyltransferase activity and the silencing function of the EED-EZH2 complex. Mol. Cell *15*, 57–67.

Creyghton, M.P., Cheng, A.W., Welstead, G.G., Kooistra, T., Carey, B.W., Steine, E.J., Hanna, J., Lodato, M.A., Frampton, G.M., Sharp, P.A., et al. (2010). Histone H3K27ac separates active from poised enhancers and predicts developmental state. Proc. Natl. Acad. Sci. USA *107*, 21931–21936.

Cui, K., Zang, C., Roh, T.Y., Schones, D.E., Childs, R.W., Peng, W., and Zhao, K. (2009). Chromatin signatures in multipotent human hematopoietic stem cells indicate the fate of bivalent genes during differentiation. Cell Stem Cell *4*, 80–93.

de Almeida, S.F., Grosso, A.R., Koch, F., Fenouil, R., Carvalho, S., Andrade, J., Levezinho, H., Gut, M., Eick, D., Gut, I., et al. (2011). Splicing enhances recruitment of methyltransferase HYPB/Setd2 and methylation of histone H3 Lys36. Nat. Struct. Mol. Biol. *18*, 977–983.

Di Croce, L., and Helin, K. (2013). Transcriptional regulation by Polycomb group proteins. Nat. Struct. Mol. Biol. *20*, 1147–1155.

Garcia, B.A., Mollah, S., Ueberheide, B.M., Busby, S.A., Muratore, T.L., Shabanowitz, J., and Hunt, D.F. (2007). Chemical derivatization of histones for facilitated analysis by mass spectrometry. Nat. Protoc. *2*, 933–938.

Goldberg, A.D., Banaszynski, L.A., Noh, K.M., Lewis, P.W., Elsaesser, S.J., Stadler, S., Dewell, S., Law, M., Guo, X., Li, X., et al. (2010). Distinct factors control histone variant H3.3 localization at specific genomic regions. Cell *140*, 678–691.

Hansen, K.H., Bracken, A.P., Pasini, D., Dietrich, N., Gehani, S.S., Monrad, A., Rappsilber, J., Lerdrup, M., and Helin, K. (2008). A model for transmission of the H3K27me3 epigenetic mark. Nat. Cell Biol. *10*, 1291–1300.

Heintzman, N.D., Stuart, R.K., Hon, G., Fu, Y., Ching, C.W., Hawkins, R.D., Barrera, L.O., Van Calcar, S., Qu, C., Ching, K.A., et al. (2007). Distinct and predictive chromatin signatures of transcriptional promoters and enhancers in the human genome. Nat. Genet. *39*, 311–318.

Jin, F., Li, Y., Ren, B., and Natarajan, R. (2011). Enhancers: multi-dimensional signal integrators. Transcription *2*, 226–230.

Jung, H.R., Pasini, D., Helin, K., and Jensen, O.N. (2010). Quantitative mass spectrometry of histones H3.2 and H3.3 in Suz12-deficient mouse embryonic stem cells reveals distinct, dynamic post-translational modifications at Lys-27 and Lys-36. Mol. Cell. Proteomics *9*, 838–850.

Kizer, K.O., Phatnani, H.P., Shibata, Y., Hall, H., Greenleaf, A.L., and Strahl, B.D. (2005). A novel domain in Set2 mediates RNA polymerase II interaction and couples histone H3 K36 methylation with transcript elongation. Mol. Cell. Biol. *25*, 3305–3316.

Kouzarides, T. (2007). Chromatin modifications and their function. Cell *128*, 693–705.

Lanzuolo, C., Lo Sardo, F., Diamantini, A., and Orlando, V. (2011). PcG complexes set the stage for epigenetic inheritance of gene silencing in early S phase before replication. PLoS Genet. *7*, e1002370.

Lee, T.I., Jenner, R.G., Boyer, L.A., Guenther, M.G., Levine, S.S., Kumar, R.M., Chevalier, B., Johnstone, S.E., Cole, M.F., Isono, K., et al. (2006). Control of developmental regulators by Polycomb in human embryonic stem cells. Cell *125*, 301–313.

Leeb, M., Pasini, D., Novatchkova, M., Jaritz, M., Helin, K., and Wutz, A. (2010). Polycomb complexes act redundantly to repress genomic repeats and genes. Genes Dev. *24*, 265–276.

Li, J., Moazed, D., and Gygi, S.P. (2002). Association of the histone methyltransferase Set2 with RNA polymerase II plays a role in transcription elongation. J. Biol. Chem. *277*, 49383–49388.

Li, B., Howe, L., Anderson, S., Yates, J.R., 3rd, and Workman, J.L. (2003). The Set2 histone methyltransferase functions through the phosphorylated carboxyl-terminal domain of RNA polymerase II. J. Biol. Chem. *278*, 8897–8903.

Loyola, A., Bonaldi, T., Roche, D., Imhof, A., and Almouzni, G. (2006). PTMs on H3 variants before chromatin assembly potentiate their final epigenetic state. Mol. Cell *24*, 309–316.

Margueron, R., and Reinberg, D. (2011). The Polycomb complex PRC2 and its mark in life. Nature *469*, 343–349.

Margueron, R., Li, G., Sarma, K., Blais, A., Zavadil, J., Woodcock, C.L., Dynlacht, B.D., and Reinberg, D. (2008). Ezh1 and Ezh2 maintain repressive chromatin through different mechanisms. Mol. Cell *32*, 503–518.

Margueron, R., Justin, N., Ohno, K., Sharpe, M.L., Son, J., Drury, W.J., 3rd, Voigt, P., Martin, S.R., Taylor, W.R., De Marco, V., et al. (2009). Role of the polycomb protein EED in the propagation of repressive histone marks. Nature *461*, 762–767.

McCabe, M.T., Graves, A.P., Ganji, G., Diaz, E., Halsey, W.S., Jiang, Y., Smitheman, K.N., Ott, H.M., Pappalardi, M.B., Allen, K.E., et al. (2012). Mutation of A677 in histone methyltransferase EZH2 in human B-cell lymphoma promotes hypertrimethylation of histone H3 on lysine 27 (H3K27). Proc. Natl. Acad. Sci. USA *109*, 2989–2994.

Mendenhall, E.M., Koche, R.P., Truong, T., Zhou, V.W., Issac, B., Chi, A.S., Ku, M., and Bernstein, B.E. (2010). GC-rich sequence elements recruit PRC2 in mammalian ES cells. PLoS Genet. *6*, e1001244.

Mikkelsen, T.S., Ku, M., Jaffe, D.B., Issac, B., Lieberman, E., Giannoukos, G., Alvarez, P., Brockman, W., Kim, T.K., Koche, R.P., et al. (2007). Genome-wide maps of chromatin state in pluripotent and lineage-committed cells. Nature *448*, 553–560.

Mohn, F., Weber, M., Rebhan, M., Roloff, T.C., Richter, J., Stadler, M.B., Bibel, M., and Schübeler, D. (2008). Lineage-specific polycomb targets and de novo DNA methylation define restriction and potential of neuronal progenitors. Mol. Cell *30*, 755–766.

Morey, L., and Helin, K. (2010). Polycomb group protein-mediated repression of transcription. Trends Biochem. Sci. *35*, 323–332.

Ong, C.T., and Corces, V.G. (2011). Enhancer function: new insights into the regulation of tissue-specific gene expression. Nat. Rev. Genet. *12*, 283–293.

Pasini, D., Bracken, A.P., Jensen, M.R., Lazzerini Denchi, E., and Helin, K. (2004). Suz12 is essential for mouse development and for EZH2 histone methyltransferase activity. EMBO J. *23*, 4061–4071.

Pasini, D., Bracken, A.P., Hansen, J.B., Capillo, M., and Helin, K. (2007). The polycomb group protein Suz12 is required for embryonic stem cell differentiation. Mol. Cell. Biol. *27*, 3769–3779.

Pasini, D., Hansen, K.H., Christensen, J., Agger, K., Cloos, P.A., and Helin, K. (2008). Coordinated regulation of transcriptional repression by the RBP2 H3K4 demethylase and Polycomb-Repressive Complex 2. Genes Dev. *22*, 1345–1355.

Pasini, D., Cloos, P.A., Walfridsson, J., Olsson, L., Bukowski, J.P., Johansen, J.V., Bak, M., Tommerup, N., Rappsilber, J., and Helin, K. (2010). JARID2 regulates binding of the Polycomb repressive complex 2 to target genes in ES cells. Nature *464*, 306–310.

Phatnani, H.P., and Greenleaf, A.L. (2006). Phosphorylation and functions of the RNA polymerase II CTD. Genes Dev. *20*, 2922–2936.

Rada-Iglesias, A., Bajpai, R., Swigut, T., Brugmann, S.A., Flynn, R.A., and Wysocka, J. (2011). A unique chromatin signature uncovers early developmental enhancers in humans. Nature *470*, 279–283.

Ringrose, L., Rehmsmeier, M., Dura, J.M., and Paro, R. (2003). Genome-wide prediction of Polycomb/Trithorax response elements in Drosophila melanogaster. Dev. Cell *5*, 759–771.

Scharf, A.N., Barth, T.K., and Imhof, A. (2009). Establishment of histone modifications after chromatin assembly. Nucleic Acids Res. *37*, 5032–5040.

Schmitges, F.W., Prusty, A.B., Faty, M., Stützer, A., Lingaraju, G.M., Aiwazian, J., Sack, R., Hess, D., Li, L., Zhou, S., et al. (2011). Histone methylation by PRC2 is inhibited by active chromatin marks. Mol. Cell *42*, 330–341.

Schoeftner, S., Sengupta, A.K., Kubicek, S., Mechtler, K., Spahn, L., Koseki, H., Jenuwein, T., and Wutz, A. (2006). Recruitment of PRC1 function at the initiation of X inactivation independent of PRC2 and silencing. EMBO J. *25*, 3110–3122.

Shen, X., Liu, Y., Hsu, Y.J., Fujiwara, Y., Kim, J., Mao, X., Yuan, G.C., and Orkin, S.H. (2008). EZH1 mediates methylation on histone H3 lysine 27 and complements EZH2 in maintaining stem cell identity and executing pluripotency. Mol. Cell *32*, 491–502.

Simon, J.A., and Kingston, R.E. (2009). Mechanisms of polycomb gene silencing: knowns and unknowns. Nat. Rev. Mol. Cell Biol. *10*, 697–708.

Sing, A., Pannell, D., Karaiskakis, A., Sturgeon, K., Djabali, M., Ellis, J., Lipshitz, H.D., and Cordes, S.P. (2009). A vertebrate Polycomb response element governs segmentation of the posterior hindbrain. Cell *138*, 885–897.

Steiner, L.A., Schulz, V.P., Maksimova, Y., Wong, C., and Gallagher, P.G. (2011). Patterns of histone H3 lysine 27 monomethylation and erythroid cell type-specific gene expression. J. Biol. Chem. *286*, 39457–39465.

Tachibana, M., Ueda, J., Fukuda, M., Takeda, N., Ohta, T., Iwanari, H., Sakihama, T., Kodama, T., Hamakubo, T., and Shinkai, Y. (2005). Histone methyltransferases G9a and GLP form heteromeric complexes and are both crucial for methylation of euchromatin at H3-K9. Genes Dev. *19*, 815–826.

Tie, F., Banerjee, R., Stratton, C.A., Prasad-Sinha, J., Stepanik, V., Zlobin, A., Diaz, M.O., Scacheri, P.C., and Harte, P.J. (2009). CBP-mediated acetylation of histone H3 lysine 27 antagonizes Drosophila Polycomb silencing. Development *136*, 3131–3141.

Vakoc, C.R., Sachdeva, M.M., Wang, H., and Blobel, G.A. (2006). Profile of histone lysine methylation across transcribed mammalian chromatin. Mol. Cell. Biol. *26*, 9185–9195.

Vella, P., Barozzi, I., Cuomo, A., Bonaldi, T., and Pasini, D. (2012). Yin Yang 1 extends the Myc-related transcription factors network in embryonic stem cells. Nucleic Acids Res. *40*, 3403–3418.

Wu, H., Chen, X., Xiong, J., Li, Y., Li, H., Ding, X., Liu, S., Chen, S., Gao, S., and Zhu, B. (2011). Histone methyltransferase G9a contributes to H3K27 methylation in vivo. Cell Res. *21*, 365–367.

Xiao, T., Hall, H., Kizer, K.O., Shibata, Y., Hall, M.C., Borchers, C.H., and Strahl, B.D. (2003). Phosphorylation of RNA polymerase II CTD regulates H3 methylation in yeast. Genes Dev. *17*, 654–663.

Yuan, W., Xu, M., Huang, C., Liu, N., Chen, S., and Zhu, B. (2011). H3K36 methylation antagonizes PRC2-mediated H3K27 methylation. J. Biol. Chem. *286*, 7983–7989.